

Measuring Cellular Structure at Submicrometer Scale With Light Scattering Spectroscopy

Vadim Backman, Venkatesh Gopal, Maxim Kalashnikov, Kamran Badizadegan, Rajan Gurjar, Adam Wax, Irene Georgakoudi, Markus Mueller, Charles W. Boone, Ramachandra R. Dasari, and Michael S. Feld

Abstract—We present a novel instrument for imaging the angular distributions of light backscattered by biological cells and tissues. The intensities in different regions of the image are due to scatterers of different sizes. We exploit this to study scattering from particles smaller than the wavelength of light used, even when they are mixed with larger particles. We show that the scattering from subcellular structure in both normal and cancerous human cells is best fitted to inverse power-law distributions for the sizes of the scattering objects, and propose that the distribution of scattering objects may be different in normal versus cancerous cells.

Index Terms—Cancer diagnosis, chromatin, fractal, light scattering, spectroscopy.

I. INTRODUCTION

THE majority of human cancers originate in the epithelial linings of the body. The diagnosis of early cancer and intra-epithelial neoplastic changes such as dysplasia and carcinoma *in situ* (CIS) has traditionally relied on the microscopic examination of differentially stained tissue samples obtained via biopsy. The most common tissue stains are hematoxylin, which stains the acidic histones and the nucleic acids within cell nuclei blue, and eosin, which stains basic proteins red. In a given tissue, the intensity of staining by hematoxylin and eosin (H&E) is a measure of the concentration of stainable solids (proteins, DNA, RNA, etc.). Enlarged and intensely stained (“hyperchromatic”) nuclei are among the most important diagnostic criteria used by pathologists to diagnose early cancerous and neoplastic transformations.

Cellular components with higher concentrations of solids also exhibit a higher refractive index [1]. When the cell is illuminated by visible light, these refractive index variations scatter light. The spectral and angular distributions of the scattered light are determined by the size and refractive index distributions of the scattering regions. Recently, a technique called light scattering spectroscopy (LSS) has been developed to exploit this phenomenon in biological tissue [2].

By measuring and analyzing light that is backscattered by the tissue after a single scattering event, the size and refractive index

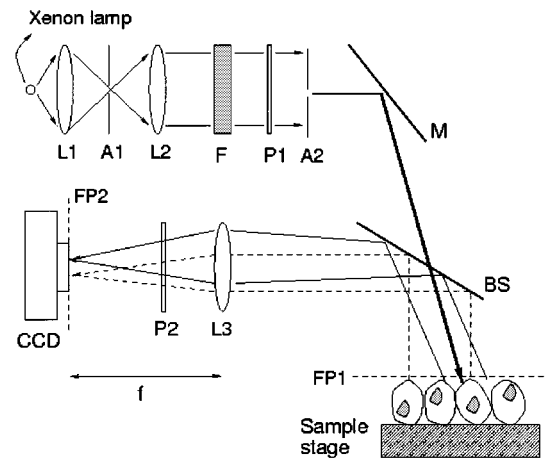


Fig. 1. A/LSS apparatus. L1, L2: collimating lenses; A1, A2: Iris diaphragms; F: narrow-band filter; P1, P2: polarizers; M: Mirror, BS: 50:50 beam splitter, CCD: 16 bit CCD camera. The sample is mounted on the sample stage.

distributions of the nuclei of epithelial cells can be determined. This provides a broadly applicable means to probe cell structure and to provide valuable diagnostic information for detection of epithelial neoplasia and early cancerous lesions in a number of optically accessible organs [3]–[7].

Cell nuclei are good targets for LSS analysis because they are the largest cellular organelles, with sizes ranging from 5 to 15 μm . They also have one of the highest indexes of refraction amongst the components of epithelial cells [8]. However, changes in size and density are not the only cell nuclear features indicative of neoplastic change. Coarse clumping of hematoxylyn-stained chromatin, the solid material within the nucleus, with a sharp optical density gradient at the borders of the clumps (“sharp margination”) and a general coarsening of the chromatin texture, have also been shown to correlate with the degree of intra-epithelial neoplasia and have been used to make prognostic assessments [9], [10]. We note that these alterations of cellular architecture and the associated changes in refractive index occur on a scale of the order of f or less than the wavelength of visible light. Here, we report a new modality of LSS, scattering angle sensitive LSS (A/LSS) that enables quantitative assessment of submicrometer scale refractive index variations in living cells and tissues.

II. EXPERIMENTAL SETUP

A schematic diagram of the apparatus is shown in Fig. 1. A beam from a broad-band xenon arc lamp (Oriel, Inc.) is spatially filtered and collimated by lenses L1 ($f = 170 \text{ mm}$), L2

Manuscript received August 10, 2001; revised October 30, 2001. This work was supported by NIH Grant P41-RR02594 and by NIH Grant R01-CA53717.

V. Backman is with the Biomedical Engineering Department, Northwestern University, Evanston, IL 60208 USA.

V. Gopal, M. Kalashnikov, R. Gurjar, A. Wax, I. Georgakoudi, M. Mueller, C. W. Boone, R. R. Dasari, and M. S. Feld are with the G.R. Harrison Spectroscopy Laboratory, Massachusetts Institute of Technology, Cambridge, MA 02139 USA.

K. Badizadegan is with the Department of Pathology, Children’s Hospital, Harvard Medical School, Boston, MA 02115 USA.

Publisher Item Identifier S 1077-260X(01)11252-9.

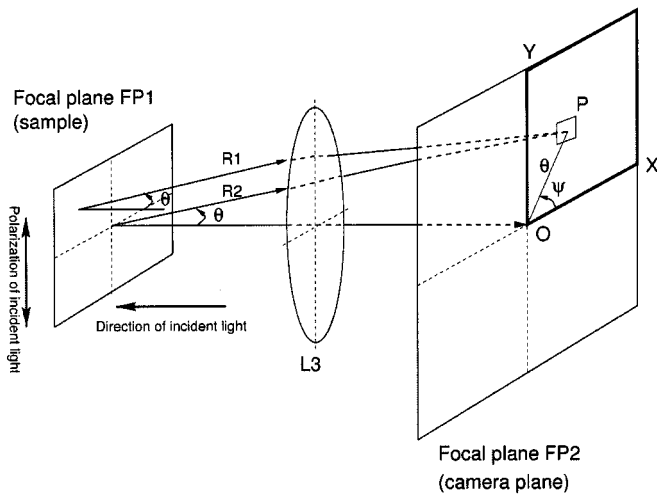


Fig. 2. Unfolded view of the optical path from the sample stage to the camera image plane. FP1 and FP2 are the front and back focal planes of the lens L3. A spatial map of the angular distribution of light scattered by the sample in the plane FP1 is formed at the camera, which is placed at the plane FP2. The scattering angle θ and the azimuth φ are indicated. Parallel rays R1 and R2 that exit the sample at the same scattering and azimuth angle are coincident at the same point in the plane FP2, shown here by the tile marked P.

($f = 95$ mm) and the aperture A1. A series of narrow-band optical filters F (Edmund Scientific, FWHM = 20 nm) with center wavelengths λ_i , selects a narrow wavelength band. In our experiments $\lambda_i = 532, 550, 568, 589, 620, 650, 671, 694$ nm. The beam is then polarized by polarizer P1, passed through a second aperture A2 which is used to reduce the diameter of the beam to about 3 mm, reflected from the mirror M, and made incident on the sample stage, on which the sample is mounted. The mirror M is set such that the beam strikes the sample stage at an angle of about 15° , which prevents the specular reflection from being imaged. The sample stage is placed at one focal plane FP1 of lens L3 ($f = 125$ mm), while a 512×512 pixel, 16 bit cooled CCD camera (Princeton Instruments, 512TK) is placed at the other focal plane FP2, where a two-dimensional (2-D) map of the angular distribution of the backscattered light is formed [11]. The polarization state of the scattered light to be viewed is selected by the analyzer P2. When P1 and P2 are parallel, the scattered intensity is denoted I_{\parallel} , whereas I_{\perp} denotes the cross-polarized intensity.

Consider an optical path from the sample stage to focal plane FP2 of lens L3, shown in Fig. 1. In Fig. 2, this path is unfolded and shown without the beamsplitter and the components are placed in a straight line. As can be seen, a 2-D map of the angular distribution of the backscattered light is formed in the camera focal plane FP2. The direction of exact backscattering is mapped onto the center of the image at O. The two rays marked R1 and R2 represent light that is scattered at polar angle θ (measured from the backward direction) and azimuth φ to the direction of exact backscattering from different parts of the sample. In Fig. 2, $\varphi = 0$ for light scattered in a direction with (x, y)-component perpendicular to the direction of polarization of the incident light x. All such parallel rays that leave the sample with identical scattering angles (θ, φ) pass through the same point, P, in the focal plane FP2. Thus, light rays scattered from all parts of the sample at a fixed angle (θ, φ) are mapped onto a fixed position in the camera image plane.

The angular and spectral distributions of light scattered elastically by a particle are determined by the size of the particle relative to the wavelength of the incident light, and by the refractive index mismatch between the particle and the surrounding medium [12]. The angular and spectral variations characterize the size and other features of the scattering particle. Broadly, there are two strategies by which particle size can be determined. The particle can be illuminated by light of a fixed wavelength and the angular variations of the scattered intensity measured. Alternatively, light can be collected from a fixed angle (θ, φ) to measure the intensity changes of the scattered light as the wavelength is varied. The technique that we employ exploits both the angular and spectral features of the scattered light.

We obtain A/LSS images of the backscattered light, i.e., intensity maps in the (θ, φ) plane, at various wavelengths and for both polarizations. For each narrow wavelength band six intensity maps are recorded. First, I_{\parallel} and I_{\perp} , the parallel and perpendicularly polarized intensities scattered by the sample, are measured. Then, the background intensity when no sample is present is measured and subtracted to remove stray illumination. Hereafter, I_{\parallel} and I_{\perp} refer to the intensities measured after stray light subtraction. Further, to correct for nonuniformities in the intensity and wavelength response of each pixel, I_{\parallel} and I_{\perp} are normalized by flat-fielding using a reflectance standard (Ocean Optics, Inc.). The corresponding (θ, φ) maps obtained with the reflectance standard are denoted I_{\parallel}^b and I_{\perp}^b , consistent with the notation in [3]. From these maps, A/LSS intensity maps, $\Delta I = (I_{\parallel}/I_{\parallel}^b) - (I_{\perp}/I_{\perp}^b)$, are calculated. These maps are formed by singly scattered light and discriminate against multiple scattering [3].

To obtain spectral information from this series of A/LSS intensity maps, a region of interest (“tile”) is selected, such as the one shown by tile P in Fig. 2. For each wavelength λ_i , the intensities of the pixels within this tile are summed. The summed intensities, plotted as a function of wavelength, yield the spectrum of the light elastically scattered into the tile. The angular range $OX = OY$ (Fig. 2) in our device is approximately 5° . Therefore, by selecting different tiles, spectral information at various scattering and azimuthal angles can be obtained. Also, the scattering is symmetric about the axes OX and OY and so it is sufficient to image only a single quadrant of the angular distribution. In Fig. 2, such a region is shown bordered by a thick solid line.

III. RESULTS

A. Experiments With Physical Models

We use polystyrene microspheres to demonstrate the properties of the A/LSS instrument. They are convenient because they have well known optical properties. The ability of LSS to measure the diameter of polystyrene beads large compared to the wavelength of light has been established previously [2]–[4]. Here we use these beads to demonstrate that the angular distribution, measured with the LSS apparatus of Fig. 1, can be used to separate the signals from large and small particles and, hence, large and small structures within cells and tissues. The polystyrene bead samples (Polysciences, Inc.) were prepared by

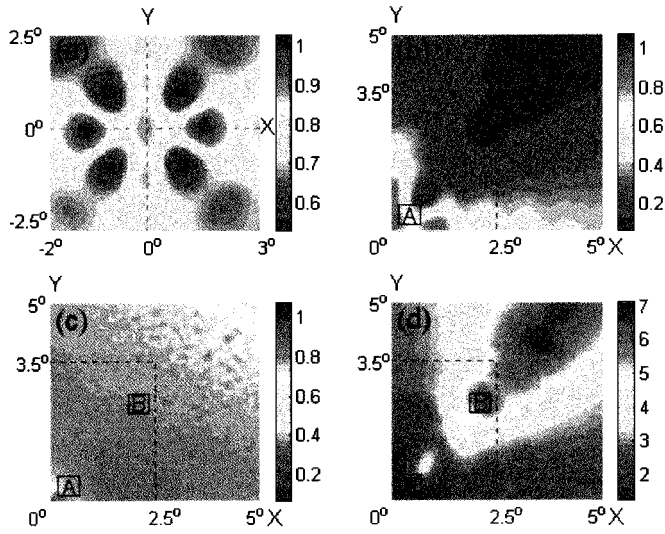


Fig. 3. (a) Parallel-polarized component (I_H) of the backscattered intensity from a suspension of 22- μm polystyrene beads, which exhibits the symmetry along two axis that makes it sufficient to image only a single quadrant for our experiments. (b) A/LSS image obtained from a suspension of 22- μm polystyrene beads. (c) A/LSS image obtained from a suspension of 0.4- μm polystyrene beads. (d) Ratio of the residual intensities (see text for details). The scattering along the x and y axes is almost entirely due to the large particles, while along the line given by $\varphi = 45^\circ$ the scattering is largely due to the smaller particles. Thus, by examining the spectra in different positions in the plane of the backscattered light, information about different size ranges can be extracted.

diluting the stock suspension with de-ionized and distilled water to obtain the required optical density.

Fig. 3 summarizes the experimental results obtained for polystyrene particles. To demonstrate the symmetry of the A/LSS scattering patterns, the parallel-polarized component $I_{||}$ of the backscattered intensity at 530 nm, scattered from a suspension of 22- μm -diameter polystyrene beads in water is shown in Fig. 3(a). The relative refractive index for polystyrene in water is ~ 1.2 . The direction of exact backscattering is at the center of the figure. The fourfold symmetry of the scattering pattern can clearly be seen. This image is in good agreement with Mie theory predictions.

In the subsequent panels of the figure, we take advantage of this radial symmetry by imaging only a single quadrant, thus increasing our angular range. In Fig. 3(b), a single quadrant of the A/LSS image ΔI backscattered by 22- μm -diameter polystyrene particles is shown, while Fig. 3(c) shows the same quantity, but from a suspension of 0.4- μm -diameter beads. It can be seen from Fig. 3(b) and (c), which are also in good agreement with Mie theory calculations, that the scattering from the large particles is strongest at $\varphi = 0^\circ, 90^\circ$, with large variations in intensity. In contrast, the scattering from the smaller particles is more uniform and is not localized to any part of the image. This suggests that examining the intensity along $\varphi = 45^\circ$, particularly for larger values of θ , provides a way to observe the scattering from smaller particles without having the signal masked by scattering from larger objects.

This observation agrees with predictions of scattering theory. In the general case of light scattering by a particle of arbitrary shape and internal structure, the scattered wave observed at a distance r and time t has amplitude components E_{s2} and E_{s1} ,

parallel and orthogonal to the plane of scattering, respectively. These components can be expressed in terms of the corresponding components of the incident wave E_{i2} and E_{i1} by means of the scattering amplitudes, $S_i(\theta, \varphi, \lambda)$, $i = 1, \dots, 4$, using matrix notation [13]

$$\begin{pmatrix} E_{s2} \\ E_{s1} \end{pmatrix} = \frac{e^{-i(\mathbf{k}\mathbf{r}-\omega t)}}{ikr} \begin{pmatrix} S_2(\theta, \varphi, \lambda) & S_3(\theta, \varphi, \lambda) \\ S_4(\theta, \varphi, \lambda) & S_1(\theta, \varphi, \lambda) \end{pmatrix} \begin{pmatrix} E_{i2} \\ E_{i1} \end{pmatrix} \quad (1)$$

where ω , \mathbf{k} , and λ are the frequency, wave-vector, and wavelength of the light, respectively. In general, the elements of the scattering matrix are functions of θ and φ . However, when the particle has axial symmetry or the observed scattering originates from an ensemble of nonsymmetrical randomly oriented particles, $S_3 = S_4 = 0$, and the only nonzero components of the scattering matrix are S_1 and S_2 , which are functions of θ , but not φ [13].

Consider a linearly polarized plane wave scattered by a particle and choose the laboratory reference system such that its axis \mathbf{x} is along the direction of polarization of the incident light. The intensities of light scattered by the particle and polarized parallel and perpendicular to the direction of polarization of the incident light are $I_{||} = |\mathbf{E} \cdot \mathbf{y}|^2$ and $I_{\perp} = |\mathbf{E} \cdot \mathbf{x}|^2$, respectively. Thus, the observed A/LSS image $\Delta I = I_{||} - I_{\perp}$ is given by

$$\Delta I = \frac{I_0}{k^2 r^2} \{ (|S_2|^2 \cos^2 \theta \sin^2 \varphi - |S_1|^2 \cos^2 \varphi) (\sin^2 \varphi - \cos^2 \varphi) - 4 \text{Re}(S_1 S_2^*) \cos \theta \cos^2 \varphi \sin^2 \varphi \} \quad (2)$$

with scattering angle θ measured from the exact backward direction. Equation (2) describes the spectral and angular distribution of the scattered light. The angular distribution depends on the size and internal structure of the scattering particles. For example, particles much larger than the wavelength of light give rise to a prominent backscattering peak in $S_1(\theta)$ and $S_2(\theta)$. The intensity profile is maximum in the backward direction (at or near $\theta = 0^\circ$) and diminishes with increasing θ . The larger the particle, the sharper the backscattering peaks and the faster the decline of their intensity with θ . Moreover, the intensity is high for $\varphi = 0^\circ$ and 90° . However, when $\varphi = 45^\circ$, the first term in (2) vanishes and the signal is proportional to the cosine of the phase shift, δ , between the complex amplitudes S_1 and S_2 (since $\text{Re}(S_1 S_2^*) \propto \cos \delta$). For a particle large compared to the wavelength, light travels long distances inside the particle and, thus, the phase shift depends strongly on θ . Therefore, $\cos \delta$ and ΔI approach zero rapidly as θ increases. Thus, the scattering by large particles is minimized at $\varphi = 45^\circ$.

On the other hand, particles with sizes comparable to or smaller than the wavelength give rise to very different scattering behavior. Because light travels shorter distances inside such particles and δ changes more slowly with θ , the scattered signal is a smooth function of θ and φ . Thus, even when large particle scattering is dominant in the backward direction, the small particle contribution can dominate for large θ and $\varphi = 45^\circ$. It is important to note that this conclusion does not require an assumption that the particles are spherical or homogenous.

To examine further whether this angular property of light scattered by large and small particles can be used to study

the light scattered by each species independently of the other, we performed the following experiment. To a suspension of 0.2–22- μm -diameter beads, particles 0.4 μm in diameter were added in an amount sufficient to equalize the contribution from large and small particles to the total optical thickness of the sample. The A/LSS image was measured before, $\Delta I_{22\ \mu\text{m}}$, and after $\Delta I_{\text{mixture}}$ addition of the small particles. Fig. 3(d) shows the ratio of the resulting images $R = \Delta I_{\text{mixture}}/\Delta I_{22\ \mu\text{m}}$. This ratio is close to one for angles near the exact backward direction [tile A in Fig. 3(d)] and along the x and y axes, which illustrates the fact that despite the addition of small particles, the backscattering signal remains unchanged in these regions. We, therefore, conclude that the scattering in these regions is dominated by the large particles. In contrast, along $\varphi = 45^\circ$ and for $\theta > 3^\circ$ [tile B in Fig. 3(d)], the contribution from the small particles dominates. Here, the intensity of light scattered by the mixture of particles is almost seven times greater than the intensity contributed by the large particles alone. Similar scattering patterns are obtained using Mie theory. This validates the strategy of observing the signal along $\varphi = 45^\circ$ to selectively observe the signal from small particles in the presence of large scatterers. Spectral information is then obtained by taking images at multiple wavelengths, λ_i , as described previously.

We emphasize that in addition to separating the contribution from small and large particles, A/LSS enables particles smaller than the wavelength of light to be sized with subwavelength accuracy. To demonstrate this, multiwavelength A/LSS images were collected for two suspensions of polystyrene beads with diameters $d = 0.4$ and $0.25\ \mu\text{m}$. After the images were collected, the spectra from angular tiles centered at $\varphi = 45^\circ$ and $\theta = 4^\circ$, which are analogous to tile B in Fig. 3(d), were obtained. The spectra predicted by Mie theory were fitted to the data using least-squares minimization. The bead diameter was chosen as the argument of the objective function, with the refractive index of the beads held fixed. The experimental data and resulting fits are shown in Fig. 4(a) and (b) for 0.4 and 0.26 μm , respectively. As can be seen, Mie theory agrees well with the experimental data. Moreover, the bead diameters that minimize the χ^2 are in good agreement with the diameters of the microspheres provided by the manufacturer, measured using a non-spectroscopic technique. We note that both samples contained beads with diameters smaller than the wavelength of light used in the experiments. Thus, A/LSS allows evaluation of the size of particles smaller than the wavelength of light. As shown below, this capability can be used to study the internal structure and organization of living cells at subwavelength (submicrometer) scale.

B. Experiments With Cells

To demonstrate the applicability of A/LSS to biological samples, we conducted experiments with substrate-attached monolayers of T84 human colon tumor cells and benign human mesothelial cells. These experiments employed a two-layered tissue model. In the upper layer, either a monolayer of T84 colon tumor cells grown on a glass coverslip or a sheet of benign mesothelial-lined peritoneum attached to a glass coverslip was placed in Hank's balanced salt solution (HBSS, Sigma Chemicals, Inc.), to simulate the epithelium. The lower layer

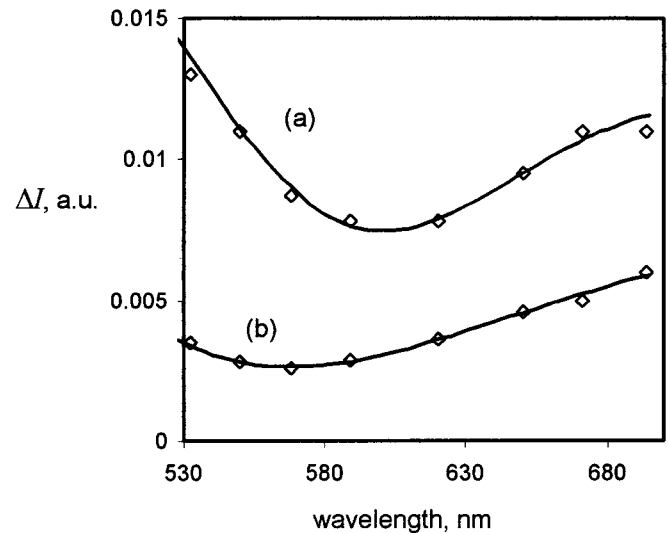


Fig. 4. Spectra of light scattered by (a) 0.4- μm and (b) 0.26- μm polystyrene microspheres. The experimental data (open diamonds) and the Mie theory fits (solid lines) are shown.

consisted of an optically thick gel containing a mixture of powdered Ba_2SO_4 and human blood. The Ba_2SO_4 mixture multiply scatters the incoming light and simulates the diffuse background due to tissue scattering. The blood simulates tissue absorption, the largest contribution to which, in the visible spectral range, is due to hemoglobin in most mucosal tissues [14]. By adjusting the concentrations of the Ba_2SO_4 and the blood, the absorption and scattering properties of the second layer were made similar to those of biological tissue [14]. In our experiments, the reduced scattering coefficient μ'_s of this layer was approximately $2.5\ \text{mm}^{-1}$ and the concentration of hemoglobin solution was 180 mg/dl.

The A/LSS images were obtained using the same procedure as in the experiments with polystyrene beads. A series of polarized images of the angular distributions of light scattered at the wavelengths λ_i listed earlier was recorded. Fig. 5(a) shows an A/LSS image of light scattered by T84 cells at 532 nm. Spectra were obtained from two regions marked A, near the direction of exact backscattering, and B, along $\varphi = 45^\circ$. Fig. 5(b) shows the spectra obtained from these two regions.

We first draw attention to the qualitative similarity between Figs. 3(b) and 5(a). The angular range observed in Fig. 5(a) is shown by the dashed line in Fig. 3(b). Two bright lobes along the axes are seen in Fig. 5(a), similar to the lobes in Fig. 3(b). Furthermore, we notice that the spectra A and B have distinct features, illustrating the difference in the origin of scattering into these angular regions. While the spectra for I_{\parallel} and I_{\perp} showed the effects of hemoglobin absorption, the A/LSS spectra of Fig. 5(b) were free of the characteristic absorption dip due to hemoglobin around 420 nm. The absence of such features indicates that subtraction of the depolarized component enables measurement of single scattered light, in agreement with our previous work on polarized light scattering [3], [6]. Spectra from regions A and B were analyzed using a Mie theory-based inversion procedure, which provides the parameters of the size distribution and refractive indexes of the scatterers that best fit the data, by comparing them against data stored in a lookup table for

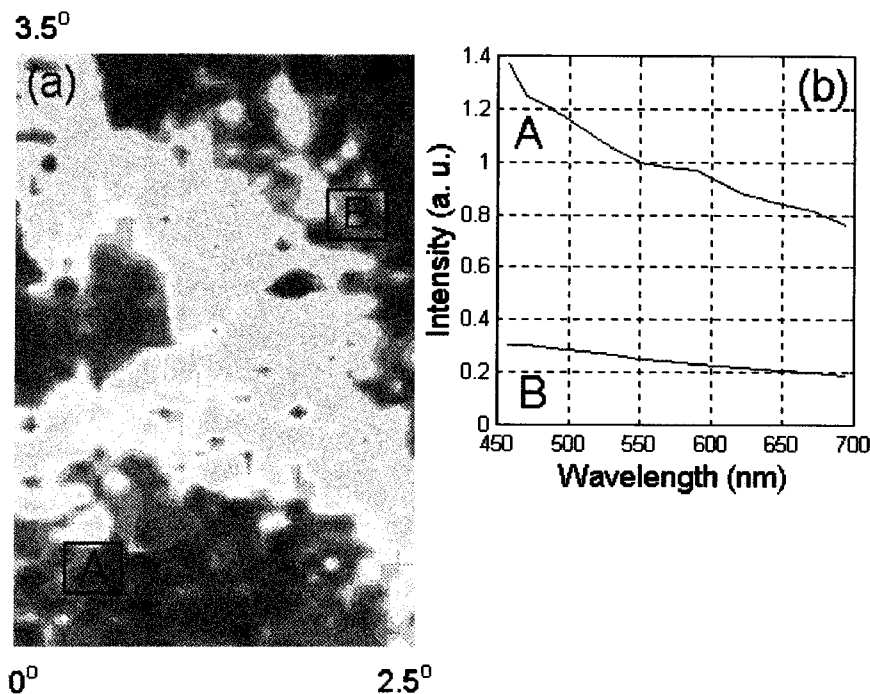


Fig. 5. Experiments with two-layer tissue models with the upper layer formed by a monolayer of T84 colon tumor cells. (a) Color-coded A/LSS contour map at $\lambda = 532$ nm. (b) Spectra of light scattered by cells in regions A and B marked on map in (a). The analysis of these spectra enables extraction of quantitative characteristics of the size distributions of scattering particles responsible for the respective scattering spectra.

various values of the scattering parameters—mean diameter and standard deviation of the size distribution of the scattering particles and their refractive index [6]. As a result of the least-square minimization, the size and refractive index parameters are found as those that minimize χ^2 .

The spectrum from region A was well fitted by a Gaussian distribution of particle diameters with a mean and standard deviation of 10.5 and 1.5 μm , respectively. As expected, this size distribution matched closely the size distribution of the largest structures inside the cells, the cell nuclei, as confirmed by morphometric measurements using a microscope after the cells were stained with H&E. The mean and standard deviation of the nuclear size distribution obtained using morphometry were 10.4 and 1.4 μm , respectively. This agrees with our previous studies showing that cell nuclei provide the major contribution to the LSS signal collected in the backward direction [2], [3], [6]. In the case of the normal mesothelial cells, the mean and standard deviation of the nuclear size distribution measured with LSS were 7.4 and 0.8 μm , respectively, close to the mean and standard deviation of 7.5 and 0.7 μm , obtained by morphometry. The larger mean and standard deviation of nuclear sizes obtained for T84 colon tumor cells agrees with the fact that these nuclei are enlarged and exhibit a greater variability in size and shape (pleomorphism). [9], [4].

In contrast to our results from region A, the spectra from region B could not be fitted under assumption that the particles are normally distributed for any mean sizes from 0.3 to 15 μm . Moreover, other types of size distributions, such as top-hat, exponential, or skewed-normal could not fit the data either. The spectra were found to be best fitted only when we used an inverse power-law distribution for the number of particles, that is, the concentration $N(d)$ of particles with a diameter d , is given

by $N(d) \propto d^{-\alpha}$, with size exponent α not dependent on d . To obtain the values of α , we used a Mie-theory based inversion procedure similar to the one discussed above. However, in this case the sizes were assumed to be distributed between 0.01 and 1.5 μm according to a power-law, with fitting parameter α . For T84 tumor cells, we found α to be approximately 2.2, whereas for normal mesothelial cells the best fit was obtained for $\alpha = 2.7$. Thus, the size distribution of the T84 colon tumor cells is shifted with respect to that of the normal cells, with an increase in the relative number of large structures.

It is interesting that the data fit suggests that the intracellular structures have a power-law size distribution. Similar distributions have been used by Schmitt *et al.* [1], [15] and Gelebart *et al.* [16] to describe particle distributions and refractive index variations in biological tissues. The choice of cutoffs of the size distributions, $0.01 \leq d \leq 1.5 \mu\text{m}$, is not critical. At small sizes, the scattering cross section scales as d^6 , whereas at large diameters, the distribution falls off sharply. Hence, the smallest and largest particles contribute only weakly to the A/LSS signals. We also recognize that although $N(d) \propto d^{-\alpha}$ provides a good fit to the data, this choice of size distribution might not be unique, since the inversion of the light scattering data is an ill-posed problem in which an entire size distribution is deduced from a finite number of data points.

IV. CONCLUSION

In summary, we have demonstrated a new modality of LSS that makes it possible to measure the size of biological particles with dimensions of the order of or smaller than the wavelength of light, even when they are present in a mixture of larger scatterers. This is possible because light singly scattered by submi-

rometer objects may be preferentially selected by measuring the signal along $\varphi = 45^\circ$. Using two layer phantoms, we also showed that polarization discrimination results in LSS signals consisting primarily of singly scattered photons. We also found that T84 tumor colon cells as well as normal mesothelial cells contain small structures with size distributions that are well described by inverse power laws. It was found that the size exponent for T84 tumor cells is smaller than that for normal mesothelial cells. This difference may be related to change in the fractal properties of the malignant cells [17]. This hypothesis is currently under study in our laboratory.

ACKNOWLEDGMENT

This work was carried out at the MIT Laser Biomedical Research Center.

The authors would like to thank Dr. D. Coffey for useful comments, and Dr. W. Lencer from the Children's Hospital, Boston, MA, for generously providing the T84 cells.

REFERENCES

- [1] J. M. Schmitt and G. Kumar, "Optical scattering properties of soft tissue: A discrete particle model," *Appl. Opt.*, vol. 37, pp. 2788–2797, 1998.
- [2] L. T. Perelman, V. Backman, M. Wallace, G. Zonios, R. Manoharan, A. Nusrat, S. Shields, M. Seiler, C. Lima, T. Hamano, I. Itzkan, J. Van Dam, J. M. Crawford, and M. S. Feld, "Observation of periodic fine structure in reflectance from biological tissue: A new technique for measuring nuclear size distribution," *Phys. Rev. Lett.*, vol. 80, pp. 627–630, 1998.
- [3] V. Backman, R. Gurjar, K. Badizadegan, I. Itzkan, R. R. Dasari, L. T. Perelman, and M. S. Feld, "Polarized light scattering spectroscopy for quantitative measurement of epithelial cellular structures," *IEEE J. Select. Topics Quantum Electron.*, vol. 5, pp. 1019–1026, July/Aug. 1999.
- [4] V. Backman, M. B. Wallace, L. T. Perelman, J. T. Arendt, R. Gurjar, M. G. Muller, Q. Zhang, G. Zonios, E. Kline, T. McGillican, S. Shapshay, T. Valdez, J. Van Dam, K. Badizadegan, J. M. Crawford, M. Fitzmaurice, S. Kabani, H. S. Levin, M. Seiler, R. R. Dasari, I. Itzkan, and M. S. Feld, "Detection of preinvasive cancer cells *in situ*," *Nature*, vol. 406, pp. 35–36, July 2000.
- [5] M. B. Wallace, L. T. Perelman, V. Backman, J. M. Crawford, M. Fitzmaurice, M. Seiler, K. Badizadegan, S. J. Shields, I. Itzkan, R. R. Dasari, J. Van Dam, and M. S. Feld, "Endoscopic detection of dysplasia in patients with Barrett's esophagus using light-scattering spectroscopy," *Gastroenterol.*, vol. 119, p. 677, 2000.
- [6] R. Gurjar, V. Backman, K. Badizadegan, R. Dasari, I. Itzkan, L. T. Perelman, and M. S. Feld, "Imaging human epithelial properties with polarized light scattering spectroscopy," *Nature Medicine*, vol. 7, pp. 1245–1248, Nov. 2001.
- [7] I. Georgakoudi, B. Jacobson, J. Van Dam, V. Backman, M. B. Wallace, M. G. Muller, Q. Zhang, K. Badizadegan, D. Sun, G. A. Thomas, L. T. Perelman, and M. S. Feld, "Fluorescence, reflectance, and light scattering spectroscopy for evaluating dysplasia in patients with Barrett's esophagus," *Gastroenterol.*, vol. 120, pp. 1620–1629, 2001.
- [8] P. M. A. Slood, "Elastic light scattering from nucleated blood cells," *Cytometry*, vol. 9, p. 636, 1988.
- [9] R. S. Cotran, S. L. Robbins, and V. Kumar, *Pathological Basis of Disease*. Philadelphia, PA: Saunders, 1999.
- [10] C. W. Boone, G. D. Stoner, J. V. Bacus, V. Kagan, M. A. Morse, G. J. Kelloff, and J. W. Bacus, "Quantitative grading of rat esophageal carcinogenesis using computer-assisted image tile analysis," *Cancer Epidemiol., Biomarkers, Prevention*, vol. 9, pp. 495–500, 2000.
- [11] E. Hecht, *Optics*, 2nd ed. Reading, MA: Addison-Wesley, 1987.
- [12] H. C. Van de Hulst, *Light Scattering by Small Particles*. New York: Dover, 1995.
- [13] R. G. Newton, *Scattering Theory of Waves and Particles*. New York: McGraw-Hill, 1969.
- [14] G. Zonios, L. T. Perelman, V. Backman, R. Manoharan, M. Fitzmaurice, and M. S. Feld, "Diffuse reflectance spectroscopy of human adenomatous colon polyps *in vivo*," *Appl. Opt.*, vol. 38, pp. 6628–6637, 1999.

- [15] J. M. Schmitt and G. Kumar, "Turbulent nature of refractive-index variations in biological tissues," *Opt. Lett.*, vol. 21, pp. 1310–1312, 1996.
- [16] G. Gelebart, E. Tinet, J. M. Tualle, and S. Avrillier, "Phase function simulation in tissue phantoms: A fractal approach," *Pure Appl. Opt.*, vol. 5, p. 377, 1996.
- [17] A. Bunde and S. Havlin, Eds., *Fractals and Disordered Systems*. New York: Springer-Verlag, 1991.



Vadim Backman received the M.S. degree from Leningrad Polytechnic Institute, St. Petersburg, Russia, in 1996, the M.S. degree in physics from Massachusetts Institute of Technology, Cambridge, MA, in 1998, and the Ph.D. degree in medical engineering and medical physics from Harvard University and the Massachusetts Institute of Technology, Division of Health Sciences and Technology, Cambridge, MA, in 2001.

He is an Assistant Professor of Biomedical Engineering at Northwestern University, Evanston, IL. His research interests include biomedical optics, spectroscopy, development of the theoretical approaches to describe light propagation in biological media, and optical diagnostic imaging.



Venkatesh Gopal received the B.Sc. in physics from the University of Madras in 1989, and M.Sc. in 1991. He received a Ph.D. in physics from the Indian Institute of Science, Bangalore, India, in 1999.

He is currently a postdoctoral fellow at the Research Laboratory of Electronics at the Massachusetts Institute of Technology, Cambridge, MA. He is working on constructing a stable atomic memory for quantum computation. His main interest is computation, especially, to understand biology from a computational perspective.



Maxim Kalashnikov received the B.S. degree from Moscow Institute of Physics and Technology, in 1999.

From 1998 to 1999, his experience included work in the field of ultrafast laser spectroscopy, and from 1999 to 2000, the study of intermolecular electron transfer in solution. He is currently pursuing the Ph.D. degree in chemistry from Massachusetts Institute of Technology. He has joined an interdisciplinary program at George R. Harrison Spectroscopy Laboratory, MIT, in January 2001. His research interests are in the study of the properties of light scattering from the "normal" and "abnormal", i.e., diseased biological tissues with the focus on the development of pre-invasive neoplastic changes in the epithelium and its effects on subnuclear and subcellular morphology.



Kamran Badizadegan received the B.S. degree in chemical engineering from MIT in 1988 and his M.D. degree from Harvard Medical School, in 1988 and 1993, respectively. He received his post-graduate training in anatomical pathology from Brigham and Women's Hospital and Children's Hospital Boston, Boston, MA.

He is currently an assistant professor of pathology at Harvard Medical School and a staff pathologist at Children's Hospital Boston. His clinical expertise, research, and teaching interests are in the areas of gastrointestinal pathology and epithelial cell biology.



Rajan Gurjar received the B.Tech. degree in engineering physics from the Indian Institute of Technology (I.I.T.), Bombay, India, and the Ph.D. degree from I.I.T., Kanpur, India, in 1998.

He is with the George R. Harrison Spectroscopy Laboratory at the Massachusetts Institute of Technology, Cambridge, MA, as a post-doctoral fellow, and has been engaged in various biomedical projects exploring the light tissue interaction using polarized light scattering techniques, and fluorescence from various DNA-protein adducts. He specializes in the

field of experimental atomic physics and nonlinear optics.



Adam Wax, received dual B.S. degrees in 1993, one in electrical engineering from Rensselaer Polytechnic Institute, Troy, NY, and one in physics from the State University of New York at Albany, Albany, NY, and the Ph.D. degree from Duke University, Durham, NC, in 1999.

He joined the George R. Harrison Spectroscopy Laboratory at the Massachusetts Institute of Technology, as a postdoctoral fellow immediately after his doctorate. As an training fellow of the National

Institutes of Health, he is engaged in research in using light scattering and interferometry to probe the biophysical properties of cells.



Irene Georgakoudi received the B.A. degree in physics from Dartmouth College, Hanover, NH, in 1993, and the M.Sc. and Ph.D. degrees in biophysics from the University of Rochester, Rochester, NY, in 1995 and 1998, respectively.

Since 1999, she has been working as an NIH postdoctoral fellow at the MIT G.R. Harrison Spectroscopy Laboratory. As a graduate student, she conducted research in the area of photodynamic therapy under the supervision of Dr. Tom Foster.

Her Ph.D. thesis involved studies of the effects of sensitizer photobleaching and localization on photodynamic dosimetry. Since her arrival at MIT, she has been working on the use of multiple spectroscopic modalities, such as fluorescence, reflectance, and light scattering for quantitative characterization of tissue biochemical and morphological features. Her interests involve the use of optical spectroscopy and imaging as tools for understanding human disease and for improving current means of disease detection and treatment.



Marcus Mueller was born in Germany. He received the Diploma in Physics from the University of Massachusetts, where he obtained an M.S. degree in Applied Physics, in 1997.

In 1997, he did research on quantum dots with near-field scanning optical microscopy at Boston University, Boston, MA. Since 1998, he has been a research scholar in the Spectroscopy Laboratory at the Massachusetts Institute of Technology. For his Ph.D. thesis, he is currently pursuing the use of fluorescence and reflectance spectroscopies in

medical diagnostics. His interests are at the intersection of physics, optics and medicine, and include the development of biomedical devices and the modeling of light propagation in tissue to detect early epithelial cancers.



Charles W. Boone received the MD degree from the University of California at San Francisco, San Francisco, CA, the Ph.D. degree in Biochemistry from the University of California at Los Angeles, Los Angeles, CA, and training in Anatomic and Clinical Pathology at UCLA, becoming an elected Fellow of the College of American Pathologists in 1985.

He practiced diagnostic pathology and family medicine at hospitals in Saudi Arabia for four years.

At the National Cancer Institute in Bethesda, MD, he was Chief of a Cell Biology Laboratory, and later a Program Director in Cancer Chemoprevention. He joined the MIT George R. Harrison Spectroscopy Laboratory as a Visiting Professor, in January, 2001. He has published over 170 papers in peer-reviewed journals, most of them dealing with cancer research at both the basic and clinical levels.



Ramachandra R. Dasari received the M.Sc. degree from the Benaras Hindu University, and the Ph.D. degree in physics from Aligarh Muslim University, in 1956 and 1960, respectively.

Until 1978, he was professor of physics at the Indian Institute of Technology, Kanpur, India, and worked at the National Research Council, Ottawa, Canada, and the University of British Columbia before joining the Massachusetts Institute of Technology, Cambridge, MA, in 1980. His current research interests include cavity QED and single

atom laser characteristics and laser spectroscopy of biomedical tissue and ultrasensitive detection of carcinogenic protein adducts.



Michael S. Feld received the S.B. degree in physics and the S.M. degree in humanities and sciences in 1963, and the Ph.D. degree in physics in 1967 from the Massachusetts Institute of Technology, Cambridge, MA.

He is a Professor of physics at the Massachusetts Institute of Technology and directs the George R. Harrison Spectroscopy Laboratory there. He conducts research in biological physics and spectroscopy. He is also active in laser physics, particularly the coherent interaction of light with

atomic and molecular systems, where his interests include cavity quantum electrodynamics, superradiance, and laser-nuclear physics. His publications include both theoretical and experimental topics. He has also done research in the history of science.